Theor. Comput. Fluid Dyn.
https://doi.org/10.1007/s00162-019-00493-z

ORIGINAL ARTICLE

Mengying Wang · Maziar S. Hemati

Detecting exotic wakes with hydrodynamic sensors

Received: 26 February 2018 / Accepted: 25 March 2019
© Springer-Verlag GmbH Germany, part of Springer Nature 2019

Abstract Wake sensing for bioinspired robotic swimmers has been the focus of much investigation owing to its relevance to locomotion control, especially in the context of schooling and target following. Many successful wake sensing strategies have been devised based on models of von Kármán-type wakes; however, such wake sensing technologies are invalid in the context of exotic wake types that commonly arise in swimming locomotion. Indeed, exotic wakes can exhibit markedly different dynamics, and so must be modeled and sensed accordingly. Here, we propose a general wake detection protocol for distinguishing between wake types from measured hydrodynamic signals alone. An ideal-flow model is formulated and used to demonstrate the general wake detection framework in a proof-of-concept study. We show that wakes with different underlying dynamics impart distinct signatures on a fish-like body, which can be observed in time-series measurements at a single location on the body surface. These hydrodynamic wake signatures are used to construct a wake classification library that is then used to classify unknown wakes from hydrodynamic signal measurements. Under ideal settings, the wake detection protocol is found to have an accuracy rate of over 95% in the majority of performance studies conducted. Further, proper tuning can lead to accuracy rates of 80% or better in low signal-to-noise environments. Thus, exotic wake detection is shown to be a viable concept, suggesting that such technologies have the potential to become key enablers of multiple-model sensing and locomotion control strategies in the future.

Keywords Wake detection · Flow classification · Bioinspired sensing · Machine learning · Vertex dynamics · Hydrodynamic signals

1 Introduction

Marine creatures display a tremendous ability to interact with their hydrodynamic surroundings: Some are able to orient themselves with respect to incoming currents [3]; some can skillfully surf wake vortices for locomotive advantage [21,22]; even the blind among them are able to school [27] and navigate obstacle-ridden waters [23,45,46]. These remarkable feats of situational awareness and hydrodynamic interaction are, in part, made possible by suitably evolved mechanosensory organs that allow these creatures to sense and perceive their hydrodynamic environments.

Communicated by Maziar S. Hemati.

M. Wang · M. S. Hemati (✉)
Aerospace Engineering and Mechanics, University of Minnesota, Minneapolis, MN 55455, USA
E-mail: mhemati@umn.edu

M. Wang
E-mail: wang5772@umn.edu

Published online: 03 April 2019

Hydrodynamic sensing modalities—such as the lateral line systems of fishes, the long facial whiskers of harbor seals, and the arrays of microsetae on the appendages of small crustaceans [6,34,40]—enable marine creatures to detect spatiotemporal patterns present in the external fluid environment. For example, the lateral line system consists of a collection of superficial and canal neuromasts distributed across an organism's body, which effectively serve as a set of directional-velocity and pressure sensors, respectively [7]. In principle, a creature can infer much information about its surroundings simply by measuring changes in the local flow; hydrodynamic signals encode and transmit information about nearby objects and flow structures. Indeed, hydrodynamic reception allows some marine swimmers to evade predators or to track prey [15,28,43].

Although it is common to associate hydrodynamic reception as a close-range sensing capability [9,32,46], the persistence of some hydrodynamic signals in the waters can allow for longer range sensing as well. For instance, the vortical wakes of swimming fish persist along the swimming path of a fish, allowing for wake detection when the relative distance between the signal transmitter and the signal receiver is large (i.e., tens of body lengths) [6]. In such instances, a passerby would be able to detect the associated hydrodynamic cues and potentially discern relevant information about another swimmer. Indeed, the hydrodynamic trails left behind by swimming fish can encode a rich amount of information about a particular swimmer and its motion. It is commonly suggested that the vortical wakes generated by marine swimmers can provide other aquatic animals with useful information about the swimmer's size, swimming speed, and even species and sex-specific information [6].

Given the astounding sensory capabilities afforded to marine creatures by hydrodynamic sensing and reception, numerous investigations have explored technological concepts for bringing hydrodynamic sensory capabilities to bear in human-engineered systems. Much effort has focused on developing artificial lateral line systems and associated strategies for various sensing and locomotion control tasks (see [40] for an excellent review of the current state of the art). For example, Chambers et al. show that vortex shedding frequency and magnitude can be used by underwater vehicles to detect a von Kármán vortex street and navigate flows with varying levels of turbulence and unsteadiness [10]. In another study, Klein and Bleckman show that having a total of two artificial lateral line canals—one on either lateral side of the body—is sufficient to discern relevant environmental information, such as object position, flow speed, and wake shedding frequency [19].

Many investigations have leveraged model-based strategies for studying higher-level hydrodynamic perception and locomotion control capabilities [11,13,14,29]. For example, DeVries et al. used an ideal-flow model to devise a lateral-line-based flow sensing strategy that fuses measurements from both velocity and pressure-based sensing modalities [13]. Experimental demonstrations of the multimodal sensing strategy show that a robot can utilize the fused hydrodynamic information for feedback control and successfully achieve rheotaxis and station-keeping [13]. In a separate study, Ren and Mohseni used an ideal-flow model to demonstrate a von Kárḿan wake sensing algorithm [29]. In their study, a mathematical model was formulated for the flow inside a canal neuromast, which was then used to demonstrate the utility of hydrodynamic reception for reconstructing the various parameters associated with a von Kármán-type wake.

An ability to sense von Kármán-type wakes is of practical interest because von Kármán-type wakes arise behind bluff bodies and many biological and bioinspired swimmers. For example, as noted in [8], carangiform swimming propulsion leads to the shedding of two single vortices per tail beat, leading to the well-known reverse von Kármán vortex street—which, as the name suggests, is simply a von Kármán wake with the vortex orientation reversed. We note here that the von Kármán-type wakes are a subclass of "2S" wakes—so-called owing to the fact that *two single* vortices are shed per cycle [44].

Despite demonstrated successes of model-based sensing and control strategies, it is important to note that the efficacy of a model-based strategy is often predicated on the reliability of the model at faithfully describing the relevant hydrodynamic interactions at play. It stands that wake sensing strategies developed in the context of von Kármán-type 2S wakes are not necessarily justified nor valid in the context of higher-order *exotic wakes*, where more than two single vortices are shed per cycle [2]. Indeed, exotic wakes are just as relevant as 2S wakes in biological and bioinspired swimming [8,18,20,24,31,33]. For instance, "eel-like" anguilliform swimming commonly leads to the shedding of two pairs of vortices per tail beat [8,41]—often called a "2P" wake owing to the *two pairs* of vortices that are shed per cycle [44]. (Note, since more than two single vortices are shed per cycle, a 2P wake constitutes an exotic wake, as originally defined [2].) Further, 2P wakes have also been associated with wake resonance modes in flapping plate experiments [24], providing a physical significance of 2P wakes as a sort of "optimal" wake type. Graphical representations of 2S and 2P patterns are shown in Fig. 2.

The existence and relevance of exotic wakes present a challenge for wake sensing, since different wake types can exhibit markedly different dynamics. This fact suggests that wake sensing strategies would benefit

from a "multiple model" approach, in which a wake is first detected and classified by type, and *then* sensed and reconstructed with a suitable model corresponding to the identified wake type. Indeed, this is one motivation for the exotic wake detection strategy that we introduce and study here.

Beyond the distinctions between 2S, 2P, and higher-order wakes, dynamical differences can also arise between various subclasses of these wake types. A familiar example is the difference between subclasses of 2S wakes: i.e., the difference between drag-producing von Kármán (vK) wakes and thrust-generating reverse von Kármán (rvK) wakes. Distinct regimes of motion also arise in exotic wakes, as has been well established in the vortex dynamics literature [2,4,36,38]. For instance, in the recent study by Basu and Stremler, an idealized point vortex model of a 2P wake was thoroughly examined and found to exhibit twelve dynamically distinct regimes of motion [4].

A careful examination of the biolocomotion literature suggests that different "wake regimes" (i.e., wakes exhibiting different dynamical characteristics) are commonly observed for a given "wake type" (i.e., a given wake pattern, such as 2S or 2P), in numerical simulations and physical experiments alike. For instance, Schnipper et al. observe *drag-producing* 2P wakes in experiments of a flapping foil [31], whereas the 2P wakes they aimed to study were motivated by the *thrust-generating* 2P wakes observed in undulatory swimming [25]. In numerical studies, Borazjani and Sotiropoulos show that anguilliform swimming can result in both drag- and thrust-producing 2P wakes [8]. Still more, the gait optimization study of Kern and Koumoutsakos suggests that an anguilliform swimming gait can be modified to achieve different objectives, but will consistently generate a 2P wake pattern, e.g., swimming to maximize velocity and swimming to maximize efficiency both yield 2P wake patterns [18]. The dynamical differences between each of these 2P wakes suggest that there may be much more information to glean from a wake signature simply by considering the wake dynamics; associating a wake signature with a particular wake regime can allow inferences about the wake-generating system. Although future work is still needed to establish connections between specific wake dynamics and various swimming characteristics [16], the study here will demonstrate that different wake regimes impart distinct hydrodynamic signatures that can enable wake detection and classification from sensor measurements. For example, a carangiform swimmer (2S wake generator) can be distinguished from an anguilliform swimmer (2P wake generator) from hydrodynamic wake signatures alone. Further, it may be possible to determine more refined information by considering the sub-regimes of motion, such as whether a particular anguilliform swimmer was swimming for speed or efficiency. In fact, we will show here that wake types and wake regimes can be classified using hydrodynamic signals measured at only a single location on the surface of a fish-like body, at least in the context of ideal fluids models. To do so, we begin by constructing a library of wake signatures from known wake types. Then, given the measured signature from an unknown nearby wake, the type and dynamical regime of the wake can be determined by comparing against entries in the library.

In this study, we explore the viability of classifying wake regimes from hydrodynamic signal measurements. Attention is restricted to 2S and 2P wakes because these wakes are well studied and because this choice allows the study to maintain a smaller parameter space for demonstration purposes. As will be shown, the protocol is able to successfully classify various 2S and 2P wake regimes. Although the protocol is demonstrated in a proof-of-concept setting using ideal fluids models for a limited set of wake types and specific type of sensor, the general wake detection framework is applicable more broadly as well.

We begin, in Sect. 2, by introducing a general framework for wake detection. Then, the remainder of the manuscript will focus on the specific details of the proof-of-concept demonstration. In Sect. 3, we present an ideal-flow model to represent the dynamics of various wakes and to study the hydrodynamic signatures that they impart on a fish-like body. In Sect. 4, we present a detailed study of the wake detection strategy in the context of the ideal-flow model. The model used here is a well-studied wake model that can be used to objectively validate and assess the performance of the protocol, owing to a clear delineation between wake types and regimes. Each step in the construction of the wake detection protocol is presented along with a performance study. Finally, in Sect. 5, we discuss the results of the study, draw conclusions, and offer suggestions for future investigations.

2 A general framework for wake detection and classification

The problem of exotic wake detection is concerned with associating measured hydrodynamic signals with a particular wake type. Indeed, the exotic wake detection problem can be framed as a problem in time-series classification, which we will address by means of a general supervised learning strategy. Ultimately, this strategy will allow an unknown wake to be detected and classified solely from measured hydrodynamic

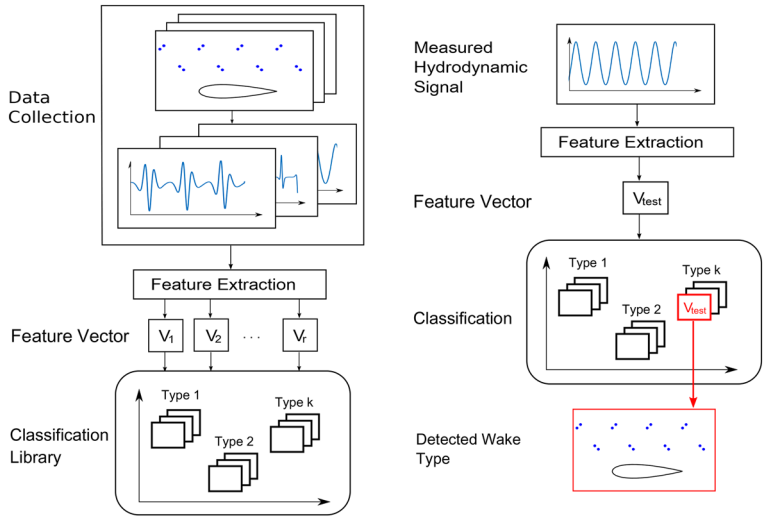

(a) Library construction **(b)** Wake Classification

Fig. 1 Synthesis of an exotic wake detection protocol consists of two primary tasks, summarized graphically here. The library construction stage in (**a**) is performed first, followed by the wake classification procedure shown in (**b**)

signals. However, before the actual classification task can be accomplished, the proposed approach will require a library of wake signatures to be constructed. In constructing this library, it is assumed that the wake types are known, such that every entry in the library of wake signatures has a wake type associated with it. In practice, one could implement an unsupervised wake regime learning scheme to construct such a library [16]. Once the library is constructed, the classification task can be carried out by comparing a measured signature from an unknown wake type with the entries in the library. In this way, the "closest match" in the library with the measured signal can be used to classify the unknown wake. Below we outline more specifically the steps that must be taken to construct a library and implement a general wake detection and classification protocol.

To construct a wake classification library, we begin by collecting sensor measurements over a large number of known wake types. In doing so, it is important to capture multiple realizations from each of the various wake types that are to be included in the library; this is needed to ensure that the library will be sufficiently rich for the classification task. Since we are working with time-series data, it will also be useful to perform a "feature extraction" step that transforms the time-series signal into a "static" feature vector, denoted V_i, such that entries in the library will be invariant to such factors as the start time of data collection. The primary challenge associated with feature extraction here rests in choosing a feature vector that adequately summarizes the time-series data and can be used to effectively distinguish between wake types. With an appropriate feature vector defined, the feature vectors for all r realizations $\{V_1, V_2, \ldots, V_r\}$ of wake signatures can be collected along with associated wake types (i.e., "labels"), and then stored in a library for use during the wake detection and classification task. The full library construction process is summarized in Fig. 1a.

Once the library of wake signatures is constructed, a classification algorithm can be applied to classify an unknown wake type from its hydrodynamic signature—called a "test signal"—by comparing with entries in the library. In order to do so, the time-series data in the test signals must be converted into a feature vector V_{test}, as was done in the library construction stage, in order to compare with entries in the library. Classification can then be performed by evaluating which library entries match most closely with V_{test}. In the present study, we make use of the k-nearest neighbor (KNN) algorithm to perform this comparison and to determine the unknown wake type, primarily owing to its simplicity [5,39]; however, this specific algorithm can be replaced by alternative classification techniques as well. The wake detection and classification procedure is summarized in Fig. 1b.

In the next section, we present an ideal-flow model that will be used to demonstrate the wake detection and classification approach in Sect. 4. The ideal-flow model will be used to generate representative wake signature data, which will inform many of the specific implementation details that were presented more generally in this section. We note here that the model is constructed with a simplifying assumption of one-way hydrodynamic coupling—with the wake influencing the body, but not vice versa—in order to maintain the integrability of the wake dynamics; indeed, this is a necessary consideration for preserving the objective definition of dynamical

regimes needed to validate the wake detection protocol in this proof-of-concept demonstration. Implementation details, such as the choice of feature vectors, will be guided by insights gained from a careful analysis of the specific wake signatures that are collected during the library construction processes.

3 Theoretical modeling

At this point, we are interested in formulating a modeling framework by which to demonstrate the wake detection and classification approach described in Sect. 2. To this end, we will formulate an ideal-flow model to represent the hydrodynamic influence of a dynamic wake on a fish-like body. We emphasize, however, that the wake detection and classification approach presented in Sect. 2 is not model based, rather, it is entirely data driven. The ideal-flow model formulated here is used only to generate representative wake signatures for the proof-of-concept studies presented in Sect. 4. In principle, the wake detection approach can be applied to generate a classification library and classify wake signatures obtained in other settings just as well, since the approach is entirely data driven. In this study, we are most interested in validating and demonstrating the performance of the approach, and so we choose to use an ideal-flow model that is best suited for this, as will be described next.

Important to the present study is the ability to generate different regimes of motion within a given wake type; beyond determining whether a wake signature is associated with a 2S or 2P wake, we will also seek to determine whether a nearby wake is a von Kármán 2S wake (vK), a reverse von Kármán 2S wake (rvK), or any of a number of 2P wake sub-regimes. To this end, we represent the ambient wake vorticity as a singly-periodic array of point vortices, whose evolution is governed by the associated vortex dynamics equations. Different wake types can be represented simply by changing the number of point vortices in the base strip, while sub-regimes can be attained by modifying physical parameters associated with the vortex system, as will be described in Sect. 3.1. These singly-periodic wake models are ideally suited for the purposes of our study here: These models allow various wakes and dynamical sub-regimes to be known ahead of time, and thus provide an objective baseline for validating the wake detection and classification approach. Further, the practical significance of these models has been suggested in previous studies of these exotic wake models [4,38].

Further, we employ a vortex panel method to model the fish-like body, as will be described in Sect. 3.2. By combining the vortex panel method with the wake dynamics model (see Fig. 4), we are able to model the hydrodynamic signatures of various wake regimes imparted on a fish-like body. A simplifying assumption of one-way coupling in the wake-body model is used to maintain integrability of the wake dynamics; that is, the model considers the hydrodynamic influence of the wake on the body, but not the hydrodynamic influence of the body on the wake evolution. The velocity at a point (or set of points) on the surface of the body can then provide time-series measurements that are representative of the hydrodynamic signals detected by a superficial neuromast or similar bioinspired velocity sensor. The modeling approach taken here can be generalized to study multiple sensing modalities. For example, the canal neuromast model of Ren and Mohseni [29] could be introduced directly—though we do not present such results here. In the present study, we focus attention to wake detection using a single velocity sensor on the surface of a fish-like body. We focus on a velocity sensor owing to its simplicity in this proof-of-concept study, but emphasize that other sensed quantities (e.g., pressure or shear-stress) could be used just as well. We find that a single velocity sensor is sufficient for the detection of ideal wakes, though introducing more sensors is expected to improve detection accuracy and robustness in non-ideal settings.

3.1 Vortex wake modeling

Here, we summarize the basic formulation of the wake dynamics models, and then discuss specific cases of 2S and 2P wakes. The vorticity $\omega(z,t)$, as a function of complex position $z = x + iy$ and time t, can be represented by a system of N point vortices,

$$\omega(z,t) = \sum_{\alpha=1}^{N} \Gamma_\alpha \delta(z - z_\alpha(t)), \tag{1}$$

where $\Gamma_\alpha \in \mathbb{R}$ and $z_\alpha(t) \in \mathbb{C}$ denote the strength and complex position of vortex α, respectively. Here, we assume that the vortex strengths remain constant in time. In the unbounded domain, a system of N point vortices evolves according to [12,26]

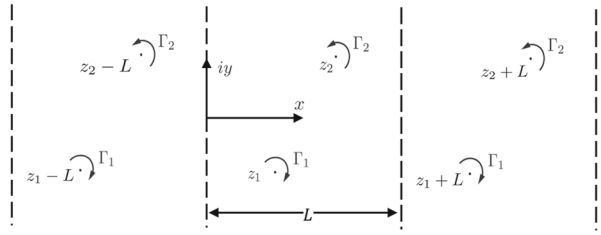

(a) Idealized 2S wake model $(N = 2)$

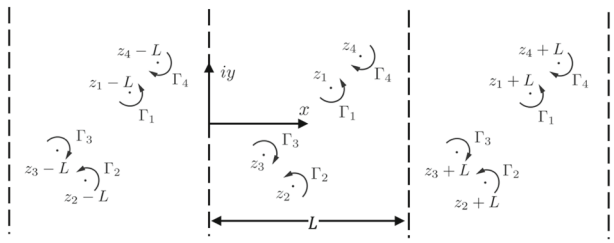

(b) Idealized 2P wake model $(N = 4)$

Fig. 2 The evolution of point vortices on a singly-periodic strip can be used to model wake dynamics. Here, three spatial periods are plotted for the point vortex models associated with **a** a 2S wake and **b** a 2P wake

$$\frac{\mathrm{d}z_\alpha{}^*}{\mathrm{d}t} = \frac{1}{2\pi i}\sum_{\substack{\beta=1\\ \beta\neq\alpha}}^{N} \frac{\Gamma_\beta}{z_\alpha - z_\beta}, \tag{2}$$

where $(\cdot)^*$ denotes complex conjugation.

In modeling the evolution of periodically shed wake vorticity, we consider the evolution of N vortices in a strip of a singly-periodic domain (see Fig. 2). Thus, we account for the mutual interactions between all the vortices in a given strip (as in Eq. 2), as well as the interactions with all of the vortices in the strips along the periodic direction (taken as x here). Taking the length of a single strip to be $L \in \mathbb{R}$, the evolution of all vorticity in the singly-periodic domain can be expressed as

$$\frac{\mathrm{d}z_\alpha{}^*}{\mathrm{d}t} = \frac{1}{2\pi i}\sum_{\substack{\beta=1\\ \beta\neq\alpha}}^{N} \sum_{\kappa=-\infty}^{+\infty} \frac{\Gamma_\beta}{z_\alpha - z_\beta + \kappa L}. \tag{3}$$

This expression can be further simplified by noting the identity $\pi \cot \pi x = \sum_{\kappa=-\infty}^{\infty}(x+\kappa)^{-1}$, which yields the equivalent expression [36],

$$\frac{\mathrm{d}z_\alpha{}^*}{\mathrm{d}t} = \frac{1}{2Li}\sum_{\substack{\beta=1\\ \beta\neq\alpha}}^{N} \Gamma_\beta \cot\left[\frac{\pi}{L}(z_\alpha - z_\beta)\right]. \tag{4}$$

Here, the vortex system is considered from a reference frame that moves with the background flow. Since the vortex strengths are assumed to be invariant, the sum of vortex strengths Γ_∞ is a constant of motion that, in an effort to model the periodic shedding of vorticity into the wake, is taken to be zero:

$$\Gamma_\infty = \sum_{\alpha=1}^{N} \Gamma_\alpha = 0. \tag{5}$$

We note that (4) can be expressed in Hamiltonian form,

$$\Gamma_\alpha \frac{\mathrm{d}x_\alpha}{\mathrm{d}t} = \frac{\partial \mathcal{H}}{\partial y_\alpha}, \qquad \Gamma_\alpha \frac{\mathrm{d}y_\alpha}{\mathrm{d}t} = -\frac{\partial \mathcal{H}}{\partial x_\alpha}. \tag{6}$$

with the Hamiltonian for the singly-periodic vortex system—a constant of motion—given as [36],

$$\mathcal{H}(z_1, \ldots, z_N; \Gamma_1, \ldots, \Gamma_N) = -\frac{1}{4\pi} \sum_{\alpha=1}^{N} \sum_{\substack{\beta=1 \\ \beta\neq\alpha}}^{N} \Gamma_\alpha \Gamma_\beta \ln \left| \sin \left[\frac{\pi}{L} (z_\alpha - z_\beta) \right] \right|. \tag{7}$$

Hence, given a set of vortex strengths Γ_α, the topology of phase space becomes fixed. Then, a particular trajectory in phase space is determined by the initial positions of the base vortices z_α. That is, the vortex strengths fix all possible dynamical regimes, while the initial vortex positions determine which among these is actually realized.

3.1.1 2S wake model ($N = 2$)

We begin by using the point vortex framework described above to model 2S wake dynamics by setting $N = 2$ (see Fig. 2a). Since the equations of motion were formulated assuming zero net circulation in the wake, it follows that the strengths of the two point vortices in each strip are equal and opposite (i.e., $\Gamma_1 = -\Gamma_2 = \Gamma$). The equations of motion for the 2S wake then reduce to

$$\begin{aligned} \frac{\mathrm{d}z_1{}^*}{\mathrm{d}t} &= -\frac{\Gamma}{2Li} \cot \left[\frac{\pi}{L} (z_1 - z_2) \right], \\ \frac{\mathrm{d}z_2{}^*}{\mathrm{d}t} &= \frac{\Gamma}{2Li} \cot \left[\frac{\pi}{L} (z_2 - z_1) \right]. \end{aligned} \tag{8}$$

Any choice of z_1 and z_2 results in a uniformly translating configuration, with the direction of translation being a function of Δx and Δy, where $(z_1 - z_2) = (\Delta x + i\Delta y)$ [35]. When $\Delta x = nL/2$ and $y \neq 0$—for some integer n, the translational velocity is purely real, and the vortices translate parallel to the wake axis. A detailed analysis of this wake model can be found in [35]. In the present study, we focus on vK and rvK configurations with $(\Delta x, \Delta y) = (L/2, 0.28L)$, which corresponds to the same configuration considered in the wake sensing studies of Ren and Mohseni [29].

3.1.2 2P wake model ($N = 4$)

The dynamics of a 2P wake can be modeled by setting $N = 4$ (see Fig. 2b). Here, we only present a summary of these models and their associated dynamics, as needed for the present investigation. Further details and discussions of the practical significance of these models can be found in the recent works by Stremler and colleagues [4,36,38].

The 2P vortex dynamics can be reduced to an integrable two-degree-of-freedom Hamiltonian system by taking the base vortex strengths and positions to be

$$\Gamma_3 = -\Gamma_1, \qquad \Gamma_4 = -\Gamma_2 \tag{9}$$

$$z_3 = z_1^* - \frac{L}{2}, \qquad z_4 = z_2^* + \frac{L}{2}. \tag{10}$$

Defining $S := \Gamma_1 + \Gamma_2$, it follows that the non-dimensional linear impulse for the base vortices $\mathcal{Q} + i\mathcal{P} = (\pi/LS) \sum_{\alpha=1}^{N} \Gamma_\alpha z_\alpha$—a quantity related to the vortex momentum [30]—reduces to

$$\mathcal{Q} = \frac{\pi}{2} (2\gamma - 1) \tag{11}$$

$$\mathcal{P} = \frac{2\pi}{L} \left[\gamma y_1 + (1 - \gamma) y_2 \right], \tag{12}$$

where $\gamma := \Gamma_1/S$. For convenience, we take $0 \leq \Gamma_1 \leq \Gamma_2$, such that $0 \leq \gamma \leq 1/2$. Then, upon defining $Z := X + iY = \pi(z_1 - z_2)/L$ as the normalized separation between the first and second base vortices, the Hamiltonian takes the form [4]

$$\mathcal{H} = \mathcal{H}(X, Y; \gamma, \mathcal{P}). \tag{13}$$

We emphasize that the components of linear impulse ($\mathcal{Q}$ and $\mathcal{P}$), the strength ratio (γ), and the Hamiltonian ($\mathcal{H}$) are all constants of motion [37]. Thus, for the idealized 2P wake model, the evolution of the associated system of point vortices can be reduced to tracking the separations between the base pairs of vortices (X and

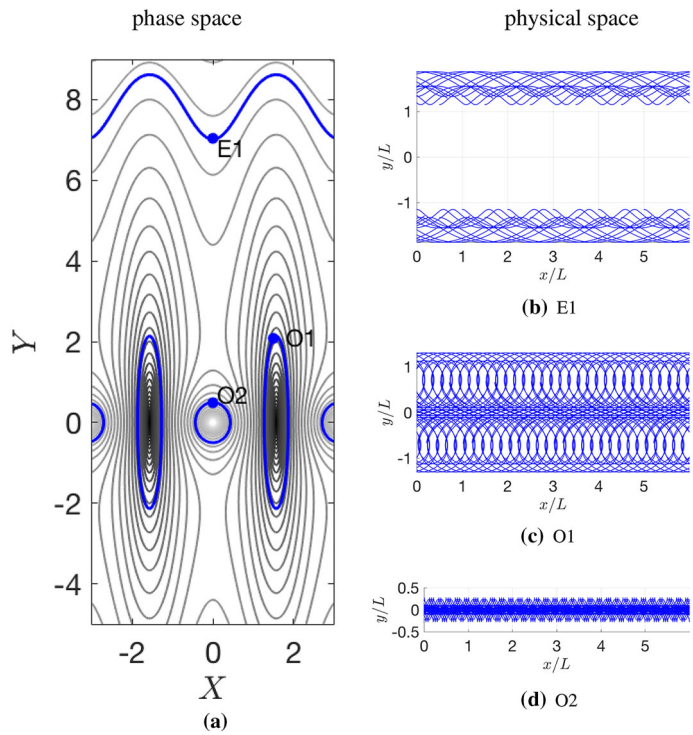

Fig. 3 Level curves of $\mathcal{H}$ define trajectories with qualitatively different behaviors in phase space (X, Y) and physical space (x, y). Representative phase-space trajectories of three wake regimes—$E1$, $O1$, and $O2$—are highlighted in (**a**), with corresponding vortex trajectories in physical space shown in (**b**)–(**d**) (colour figure online)

Y). Further, the motion is parameterized by the linear impulse of the base pairs, though it is more convenient to express this parameterization in terms of the non-dimensional strength γ and the vertical component of linear impulse $\mathcal{P}$. As shown in [4], γ and $\mathcal{P}$ constitute two independent parameters that can be chosen to realize different regimes of motion within the 2P wake model.

As shown in [4], the idealized 2P wake model can exhibit twelve distinct regimes of motion, each characterized by different patterns in the vortex trajectories. In particular, Basu and Stremler identify numerous subclasses of orbiting, exchanging, passing, scattering, and mixed patterns in the vortex trajectories. Figure 3 shows level curves of the Hamiltonian for a 2P wake with $\gamma = \frac{3}{7}$ and $\mathcal{P} = 0$ in tile (a), which corresponds to all possible phase-space trajectories. We highlight three regimes for this particular wake: an exchanging regime ($E1$) and two orbiting regimes ($O1$ and $O2$). Representative vortex trajectories of each regime in physical space are shown in tiles (b)–(d) of Fig. 3, with the corresponding phase-space trajectories highlighted in tile (a). From the figure, it is clear that each wake regime has a distinct pattern in phase space and in physical space. Our goal in the present investigation will be to distinguish between these patterns from corresponding hydrodynamic signal measurements.

As noted in the work of Stremler and colleagues in [4], the $E1$, $O1$, and $O2$ regimes correspond to "typical" (practically relevant) motions. For instance, the $O1$ regime was matched to experimentally observed patterns of a physical vortex wake in [38]. Indeed, unlike other regimes, $E1$, $O1$, and $O2$ arise over a broad range of values for the wake parameters $(\gamma, \mathcal{P})$. Scattering and passing wakes only arise in limiting cases with $\gamma = 0$ and $\gamma = 1/2$, respectively. The mixed wake regime consists of elements of both orbiting and exchanging motions, which is expected to be a difficult edge case and will not be considered here. Thus, in the current study, we will only consider the more typical $E1$, $O1$, and $O2$ regimes for 2P wakes, which will be generated over a range of $(\gamma, \mathcal{P})$ values.

3.2 Fish-like body modeling

The fish-like body in this study is modeled as a bound vortex sheet by means of a vortex panel method [17]. Here, the bound vortex sheet is represented as a set of point vortices that is appropriately distributed along

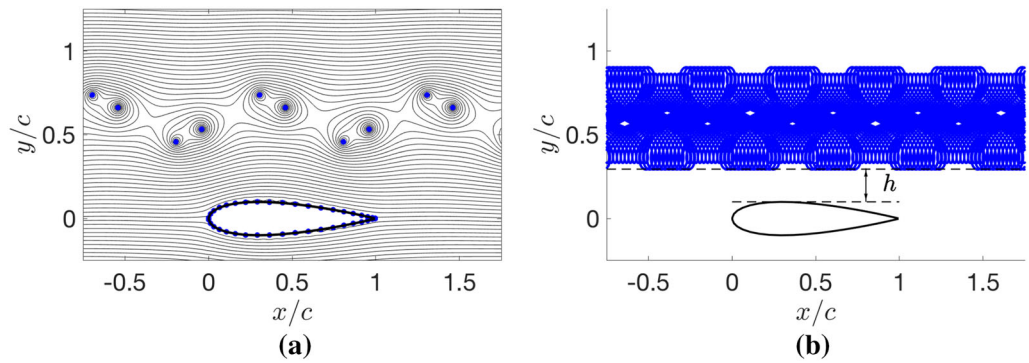

Fig. 4 A snapshot of a 2P wake in the vicinity of a fish-like body is shown in (**a**), and the associated wake-vortex trajectories are plotted in (**b**). In (**a**), free and bound point vortices are depicted as blue dots. In (**b**), blue curves depict the vortex trajectories associated with the same 2P wake in (**a**), with $\gamma = 3/7$ and $\mathcal{P} = -0.605$. The minimal lateral separation h between the wake vortices and the body is defined as in (**b**) (colour figure online)

the body surface. Further details on vortex panel methods can be found in standard texts, such as [17]. Many variations of panels methods can be found in the literature. Here, we summarize specific details of a simple variant that is used in this study.

The vortex panel method discretizes a body into P panels. Two points on each panel p are of particular interest: (1) The panel quarter-chord point will correspond to the location of a point vortex with unknown strength Γ_p^{panel} (i.e., the point at which the panel's bound vorticity is confined), and (2) the panel three-quarter-chord point will represent the point at which the no-flow-through boundary condition will be imposed (i.e., the "control point"). Note that the lumped vortex panel method enforces the Kutta condition by construction, since the circulation at the trailing edge is always exactly zero. Further, Kelvin's circulation theorem is enforced through the presence of a "starting vortex" with strength $(-\sum_{p=1}^{P} \Gamma_p^{\text{panel}})$ that resides in the far field. In the present development, the only external flow influences to be considered are the freestream velocity $\mathbf{U}_\infty$ and the velocity induced by a nearby wake $\mathbf{U}_{\text{wake}}$. Taking $\mathbf{U}_\infty$ and $\mathbf{U}_{\text{wake}}$ to be evaluated at each of the control points $(x_{\bar{c}}, y_{\bar{c}})$, we impose the flow tangency condition at each control point:

$$\sum_{p=1}^{P} a_{\bar{c}p} \Gamma_p^{\text{panel}} = -\left(\mathbf{U}_\infty + \mathbf{U}_{\text{wake}}\right) \cdot \hat{n}_{\bar{c}}, \tag{14}$$

where $\hat{n}_{\bar{c}}$ is the outward unit normal vector at control point $\bar{c}$ and

$$a_{\bar{c}p} = \frac{\Gamma_p^{\text{panel}} \left(y_p - y_{\bar{c}},\ x_{\bar{c}} - x_p\right)}{2\pi \left((x_{\bar{c}} - x_p)^2 + (y_{\bar{c}} - y_p)^2\right)} \cdot \hat{n}_{\bar{c}} \tag{15}$$

is an "influence coefficient" that represents the normal velocity induced on control point $\bar{c}$ due to unit bound circulation on panel p. The panel strengths Γ_p^{panel} can be determined by solving the system of P linear equations in (14). An example of streamlines generated by the combined wake-body model is shown in Fig. 4. Note that we assume the swimmer is coasting here, and so have not included the influence of body motions in our formulation; such considerations can be included by appropriately modifying the right-hand side of Eq. (14), and may improve detection in practice [1].

We now describe how to determine the velocity $\mathbf{U}_{\text{wake}}$ induced by a nearby vortex wake on each control point. For each vortex α among the N in the strip, denote the position as $z_\alpha = x_\alpha + i y_\alpha$ and the strength as Γ_α. Then, the velocity induced by the singly-periodic system of point vortices at the control point $(x_{\bar{c}}, y_{\bar{c}})$ is given by

$$\mathbf{U}_{\text{wake}} = \sum_{\alpha=1}^{N} \frac{\Gamma_\alpha \left(-\sinh(\Delta y_\alpha),\ \sin(\Delta x_\alpha)\right)}{2L \left(\cosh(\Delta y_\alpha) - \cos(\Delta x_\alpha) + \epsilon\right)} \tag{16}$$

where $\Delta x_\alpha = \frac{2\pi}{L}(x_{\bar{c}} - x_\alpha)$, $\Delta y_\alpha = \frac{2\pi}{L}(y_{\bar{c}} - y_\alpha)$, and ϵ is a regularization parameter that is used to ensure smoothness of solutions. As the wake evolves according to (4), the induced velocity $\mathbf{U}_{\text{wake}}$ at each control point

will change accordingly, and is thus a function of time. As such, the panel strengths will also be a function of time and (14) must be solved at each time step. In combining the vortex panel method with the idealized wake models, we have assumed that the wake induces a velocity on the body, but that the body does not alter the wake dynamics. We employ this simplifying assumption in order to preserve the integrability of the wake models, thus ensuring that the model remains suitable for objective validation of the wake detection protocol.

The time-varying nature of the hydrodynamic signature on the fish-like body will be leveraged to detect and classify wake regimes. According to the recent review in [40], most of the research and development of bioinspired hydrodynamic reception systems has focused on structures based on the superficial neuromast, which effectively measure local velocities. In the remainder of the study, we will focus on time-series measurements of local velocity at a single control point on the fish-like body. For the wake detection and classification task, we will work with a signal U' that corresponds to the velocity at a specified control point with the tangential component of the freestream velocity subtracted out. Subtracting the tangential component of the freestream from the raw signal allows the sign of the velocity induced by a nearby wake to be used for more refined discrimination between wake types, and can be used to distinguish between, e.g., vK and rvK wakes, as will be discussed in more details later.

4 Results: wake signatures and classification

With the ideal-flow model established in Sect. 3, we are ready to construct a library of wake signatures and assess the efficacy of the wake detection and classification protocol.

4.1 Wake signatures and measured hydrodynamic signals

In this study, a NACA 0020 airfoil with chord length c is used to model a fish-like body. The airfoil is represented by a total of $P = 40$ vortex panels. The dynamic wake-body simulations are performed with a fourth-order Runge–Kutta time-marching scheme; sensor measurements are sampled uniformly every 10^{-4} convective time units. In all the results presented, the measured hydrodynamic signal U' at a control point corresponds to the tangential component of local velocity with the tangential component of the freestream removed. Unless otherwise stated, the sensor measurements U' are taken at a single point on the mid-chord on the wake side of the body. Looking ahead to the feature extraction procedure, we note that the relative timescales of the wake evolution and $\mathbf{U}_\infty$ can greatly influence performance in practical applications. In principle, the signal U' must capture at least one period of wake evolution in order to perform reliable feature extraction. Here, we consider a slowly coasting body, such that multiple periods of wake evolution are available for measurement within a single convective time unit. In principle, one could simply wait longer to ensure that multiple periods of evolution are captured in the signal U'. However, doing so is typically not justified, since wake vortices can dissipate due to viscous diffusion, ultimately limiting the amount of information that can be used for feature extraction.

A total of 200 different wake realizations are simulated to build up the library and to subsequently assess the performance of the wake detection protocol. Multiple realizations of wake signatures are collected from each of the 2S (i.e., von Kármán (rvK) wakes and reverse von Kármán (rvK) wakes) and 2P wake regimes (i.e., E1, O1, and O2). For the study at hand, we take care to ensure that some consistency is maintained between the different wakes that are considered. Wake parameters are chosen such that all 2S and 2P wakes have vortices with comparable strengths. All 2P wakes are generated with $\gamma = 3/7$ and $\mathcal{P} \in \{0, -0.55, -0.605, -0.71, -0.803, -0.85, -0.9, -0.95\}$, such that the practically relevant $E1$, $O1$, and $O2$ regimes are realizable [4,38]. In order to realize 2S wakes with comparable strengths to these 2P wakes, vK and rvK wakes are constructed with $|\Gamma| \in [0.3, 0.5]$.

Further, the lateral separation between the wake and body must be consistent, in order to draw a fair comparison; otherwise, some signatures may be stronger or weaker by virtue of this geometric parameter, rather than by the nature of the wake dynamics. To this end, we also note that the vortex trajectories of 2P wakes lead to a time-varying lateral separation between the wake vortices and the body axis; thus, the separation between the wake axis and the body axis may not be the most relevant parameter to keep fixed between realizations if an objective assessment is desired. Instead, we define h to be the minimal lateral separation achieved between wake vortices and the body axis, over the course of the wake evolution (see Fig. 4).

Representative time-series measurements U'—normalized by the absolute value of the time-averaged signal $|\overline{U'}|$—for the different wake regimes with $h = 0.2L$ are shown in Fig. 5. With the exception of vK and

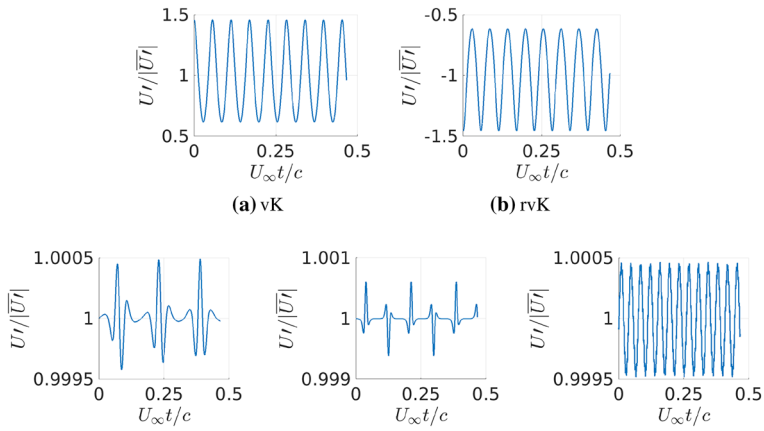

Fig. 5 Sensor signals U' have notable qualitative differences between different wake regimes. The representative signals shown here correspond to **a** $\Gamma = 0.4$, **b** $\Gamma = -0.4$, and **c–e** $\gamma = 3/7$, $\mathcal{P} = -0.803$ with $\mathcal{H} = -0.2$, 0.4, and 0.13, respectively

rvK wakes, the signals appear to be qualitatively different from one another; indeed, the signals appear to have different frequency content. This suggests that a feature vector based on a frequency-domain representation of the signal may be well suited for the classification task. In the case of vK and rvK, the sign of U' can be used to distinguish between these wakes, as will be discussed later. In the next section, we describe a specific feature extraction method that can be used to build up an effective wake classification library.

For the purposes of the present study, h is assumed to be known. As we will see, the set of features that will be used for classification will be the same regardless of the separation h, though quantitative differences will arise. As such, with h given, the protocol can switch between classification libraries to determine the wake type. An attempt was made to determine h directly from the wake signature data; however, the fish-like body in this study is taken to be in a purely coasting configuration, making the parameter h unobservable. It is expected that appropriately designed kinematics can be used to improve classification performance, even enabling h to be determined within the protocol. Indeed, the modeling framework and detection protocol can be extended to include arbitrary body kinematics, and such considerations will be the subject of future investigations.

4.2 Feature extraction from frequency-domain signatures

As seen in Fig. 5, different wake regimes impart distinct hydrodynamic signatures on the body, which can be characterized by differences in frequency content. To verify this, we compute the frequency spectra of each signal in Fig. 5 by means of a fast Fourier transform (FFT). Prior to performing the FFT, the mean signal is subtracted in order to avoid a frequency peak at zero and to facilitate the proposed feature extraction. Note that frequency content can also be efficiently computed online using short-time Fourier analysis when the sensor measurements are in the form of a datastream, as is needed in practical real-time applications [42]. The frequency-domain representations of each of these representative signals, shown in Fig. 6, show qualitative differences between each wake regime as well—again with the exception of the vK and rvK wakes. For example, 2S wakes exhibit a single dominant frequency with a large amplitude, whereas 2P wakes are more broad banded; this feature alone can be enough to distinguish a 2S wake from a 2P wake.

The frequency-domain representation is a convenient one compared to the time-domain representation of the signal for wake detection because—all else equal—it is less sensitive to implementation details, such as measurement start time. Thus, we will extract feature vectors from each signal's frequency-domain representation. The frequency signatures in Fig. 6 each display a distinct "bell" shape. Thus, we choose to summarize the frequency-domain signatures by fitting a Gaussian bell curve,

$$F(x) = a \exp\left(-\frac{(x-\mu)^2}{2\sigma^2}\right). \tag{17}$$

Note that the specific shape of the Gaussian bell curve is fully defined by the parameters (μ, a, σ), which are determined by the fitting procedure. An example is shown in Fig. 7. A feature vector for each wake realization i can then be defined using the parameters of the associated best-fit Gaussian bell curve:

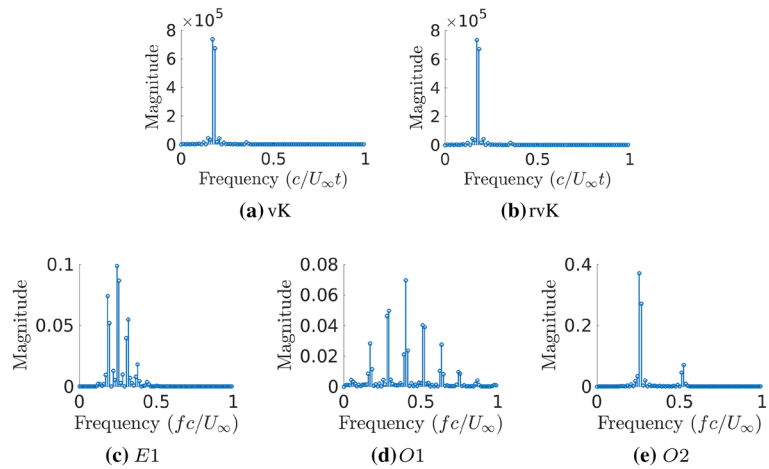

Fig. 6 Different wake regimes impart distinct signatures on the fish-like body, which can be seen in the frequency domain. The frequency-domain signatures shown here correspond to spectra from the corresponding plots in Fig. 5

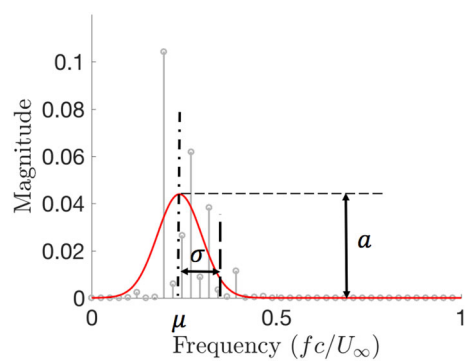

Fig. 7 A Gaussian fit to the frequency signature yields a convenient, concise, and effective set of parameters (μ, a, σ) for use as a feature vector in the wake classification task (see Eq. 17). The example plotted here corresponds to the $E1$ signature in tile (c) of Fig. 6. The parameters of the best-fit Gaussian bell curve (drawn in red) concisely summarize this signature as a feature vector (colour figure online)

$$V_i = (\mu_i, a_i, \sigma_i). \tag{18}$$

In the next section, we use the feature vector defined in (18) to build up a classification library for wake detection, but first it is worth investigating the influence of sensor location and separation distance h on the measured signals and the resulting feature vectors. For a fixed separation h, one might suspect that sensor signals will vary significantly from one measurement location to another, especially for the more complicated wake signatures of regimes $E1$ and $O1$; however, a qualitative comparison of the time-series signals from different sensor locations reveals only slight differences. Figure 8 shows the comparison of hydrodynamic signals imparted by $E1$ and $O1$ wake regimes measured at the mid-chord ($x/c = 0.5$), the maximum thickness point ($x/c = 0.2$), and the leading edge ($x/c = 0$) when $h = 0.2L$. The frequency-domain signatures and associated feature vectors are included as insets to Fig. 8. Although the feature vectors will have quantitative differences between them, the qualitative similarity between feature vectors indicates that our proposed feature extraction approach is an appropriate one regardless of sensor location. For brevity, in the remainder we only present results for the mid-chord sensor location $x/c = 0.5$.

Finally, we consider the influence of the minimal separation h on the wake signatures, and thus on the choice of features for classification. As seen in Fig. 9, the qualitative nature of the wake signatures remains relatively consistent between h values. The primary difference is in the magnitude of the spectra, which will lead to differences in the element a of each feature vector. However, the other two elements of the feature vector (i.e., μ and σ) appear to be insensitive to h, suggesting that an appropriate normalization procedure for a may extend the capabilities of the protocol for arbitrary h. Indeed, if such a procedure can be made independent of

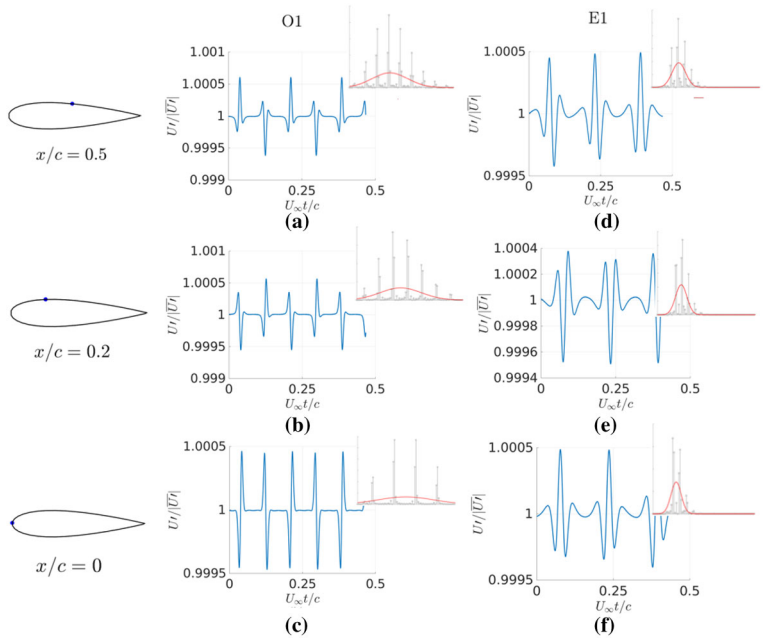

Fig. 8 Wake signatures measured at different locations along the fish body are qualitatively similar. Time- and frequency-domain signatures and corresponding feature vectors are presented for $E1$ and $O1$ wakes at the three sensor locations shown. The $E1$ and $O1$ wake signals are generated based on the same wake parameters used in Figs. 5 and 6

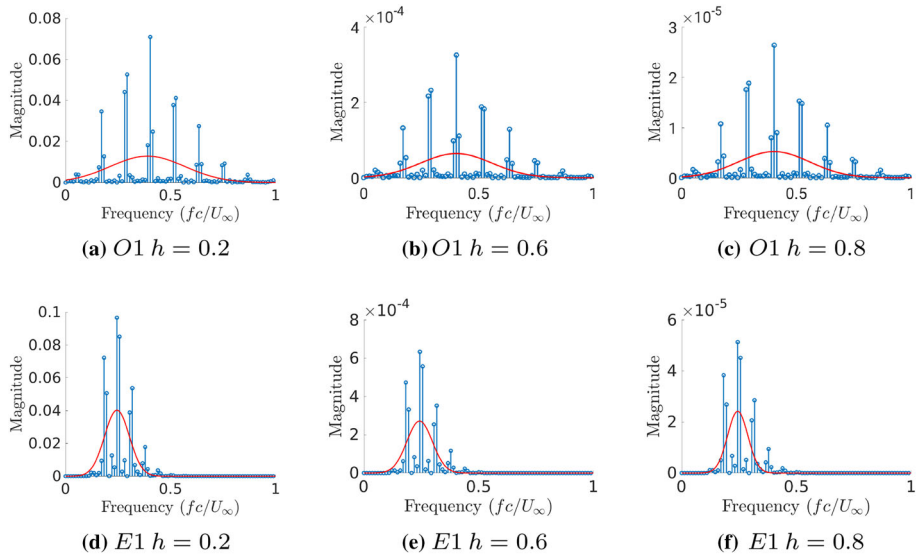

Fig. 9 Frequency domain comparison of sensor measurements simulated with different value h. The measurements are simulated at the mid-chord sensor location

h, then this would preclude the need to determine h ahead of time. In the remainder of the present study, we assume $h = 0.2L$ is known.

4.3 Wake classification

At this point, a classification library can be built up using the feature vectors defined in (18). The library is constructed by collecting an equal number of distinct feature vectors from each wake regime. The classification

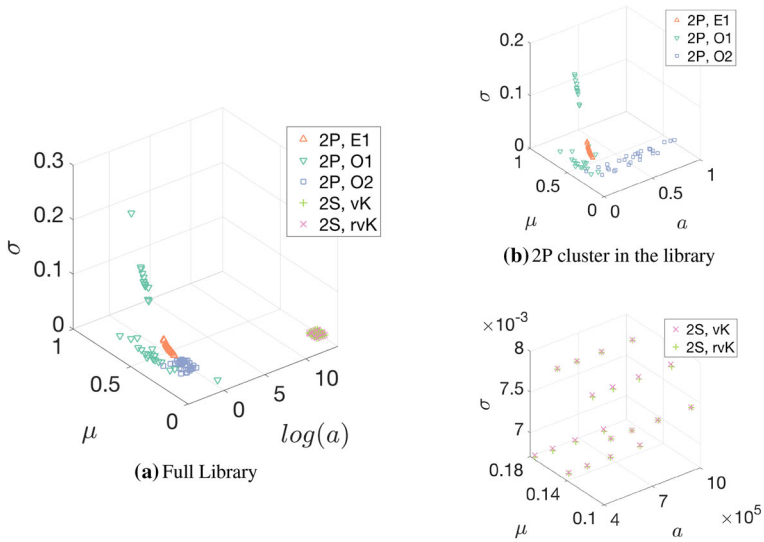

(a) Full Library

(b) 2P cluster in the library

(c) 2S cluster in the library.

Fig. 10 The wake classification library is built up in feature space with library entries from many wake types and regimes. In (**a**), an example of a classification library with a total of 150 entries is presented, equally distributed between the five regimes considered. The 2S and 2P wakes separate into distinct clusters here. A blown-up plot of the 2P and 2S clusters is shown in (**b**, **c**), respectively. Note that the 2P regimes are fairly well separated, whereas the 2S regimes are blended together (colour figure online)

library with 150 entries is presented in Fig. 10. We will report on the influence of "training size" (i.e., the number of library entries) on classification outcomes momentarily.

A quick study of Fig. 10 reveals that 2S and 2P wake types are fully partitioned into distinct clusters in feature space. A closer look at the 2P clustering in Fig. 10b shows that the various 2P wake regimes also partition relatively well, though some overlap between wake regimes is observed. Interestingly, many of these overlapping points correspond to wake signatures generated close to regime boundaries. In contrast to the 2P wake regimes, the partitioning of the vK and rvK configurations of 2S wakes do not partition as nicely (see Fig. 10c)—as is expected based on our previous observations of the associated signatures in both the time and frequency domain.

As mentioned in the development of the general wake detection framework of Sect. 2, once a library of feature vectors is available, numerous alternative classification algorithms can be applied to determine the likelihood that the signature from an unknown wake belongs to a particular class of wakes stored in the library. Here, we make use of the relatively simple k-nearest neighbor (KNN) algorithm [5,39]. Given a user-specified value k, the KNN algorithm uses a distance measure to determine which k entries among the set of all library entries $\{V_1, V_2, \ldots, V_r\}$ are closest to the test vector V_{test}. Once the k nearest neighbors have been determined, a majority voting procedure is used to assign a label to the test vector; that is, the unknown wake is determined to belong to the same class as the most frequent class among the set of k nearest neighbors. In the present study, we use the Euclidean distance as a measure of distance for the KNN algorithm; this assumes that each element of a feature vector has an equal contribution to characterizing a wake regime. Although the choice of weighting can be treated as a tuning parameter, we find that equal weightings yield adequate performance here.

We show a simple example of the KNN classification procedure at play in Fig. 11. Here, the test vector is denoted with a black $\times$, and the $k = 5$ nearest neighbors are circled in red. For the example shown, all $k = 5$ nearest neighbors correspond to $O1$ wakes, and thus, the measured hydrodynamic signal is determined to also be an $O1$ wake.

We now return to the issue of "blended" clusters of vK and rvK feature vectors. Based on the feature vectors presented in the library, it appears that vK and rvK will be virtually indistinguishable from one another. However, noting the strong separation between 2S and 2P type wakes (note the logarithmic scale of a), we can say with reasonable confidence that a 2S wake can be distinguished from a 2P wake. Thus, once a wake is classified as 2S, we can invoke an additional criterion to determine whether that particular 2S wake is vK or rvK. Since the primary distinction between vK and rvK wakes is the configuration of oppositely signed vortices, we can expect that the sign of the time-domain measurements U' will be opposite between vK and rvK wakes. Indeed, this happens to be the case in general (see Fig. 5 for one example), and so if a wake is

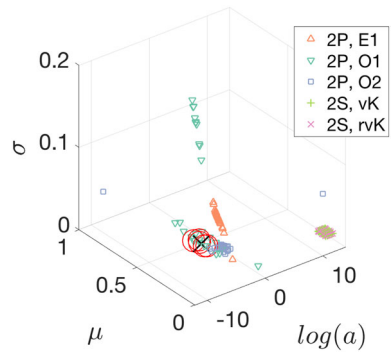

Fig. 11 An example of the wake library from Fig. 10 used for classification with a KNN algorithm applied to a test signal (denoted by ×). The $k = 5$ nearest neighbors are circled. The test signal is correctly classified as $O1$ in this example

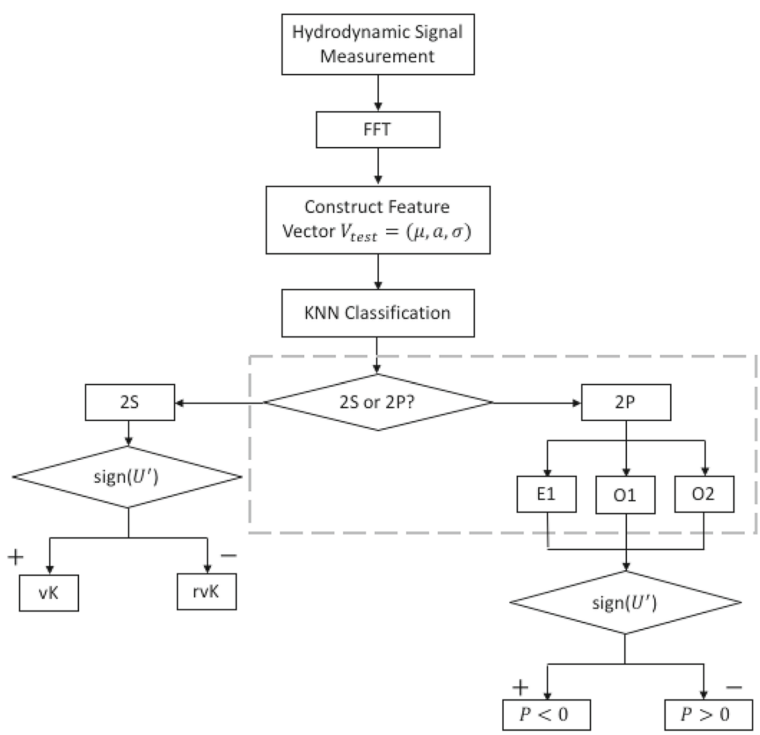

Fig. 12 A summary of the wake detection protocol used in this study

determined to be of the 2S type by the KNN classification procedure, an additional step is required to check the sign of U' to determine whether the 2S wake is vK or rvK. A similar procedure can be used to determine whether a classified 2P wake type corresponds to $\mathcal{P} > 0$ or $\mathcal{P} < 0$, though in the present study we only consider the $\mathcal{P} < 0$ case. The full wake detection and classification scheme is summarized in Fig. 12.

In the remainder of this section, we aim to assess the performance of the wake detection and classification approach described above. We are primarily interested in the classification accuracy rate, which can be quantified by applying the method to a number of "test signals" with known wake regimes. Then, the accuracy rate can be defined as the fraction of correctly classified test signals over the total number of test signals. However, since the accuracy rate will be influenced by various parameters, such as the number of nearest neighbors k and the number of entries in the classification library, robustness of accuracy rate to these parameters is the better measure of performance.

Figure 13 shows the accuracy rates corresponding to these different protocol parameter values. In this study, a total of 50 test signals were realized by drawing from a random set of 2S and 2P wake models, each constructed in a manner consistent with the generation of library entries (i.e., adhering to the same parameter

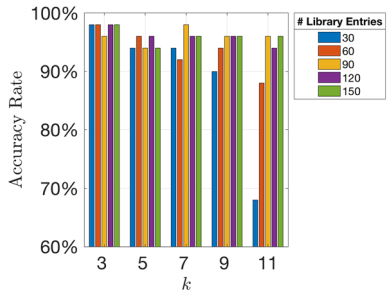

Fig. 13 A study of accuracy rate as a function of algorithm parameters reveals that the wake detection protocol has good performance. The number of nearest neighbors k and the number of library entries are both varied in this study. Accuracy rate is measured based on 50 test signals from randomly generated wakes, and is defined as the number of correct classifications over the total number of test signals

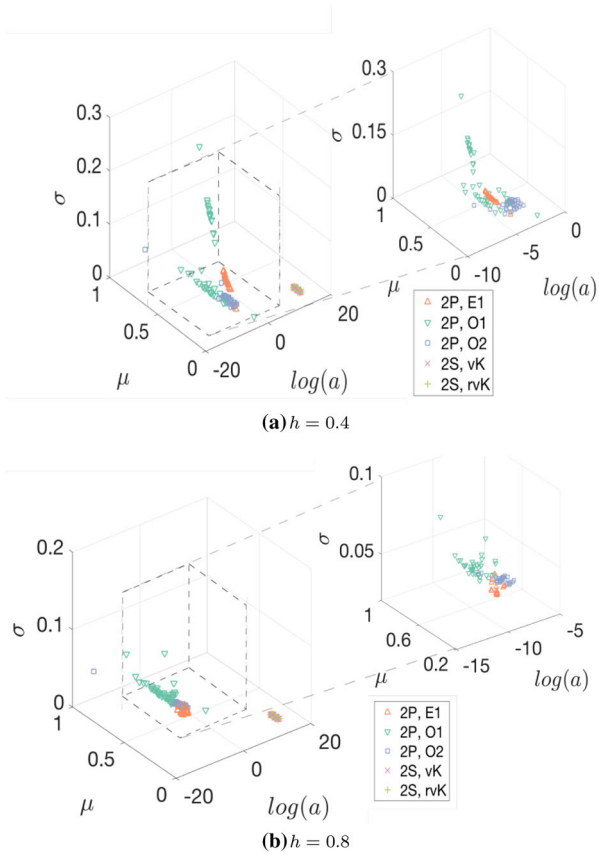

Fig. 14 As h increases, the 2P sub-regimes begin to blend together in feature space (note the logarithmic scale of a). Nonetheless, wake types 2S and 2P remain well partitioned in feature space as h increases (Refer to Fig. 10 for $h = 0.2$)

ranges and constraints). The accuracy rate of the wake detection method for the 50 test signals considered varies from 68 to 98%, depending on k and the number of library entries. The worst accuracy rate of 68% corresponds to the case with the smallest number of library entries and the largest number of nearest neighbors, as is to be expected. When the number of nearest neighbors k exceeds the number of library entries for a given wake class, it stands that "out-of-cluster" library entries will necessarily be included within each evaluation, thus degrading the classification performance. This point highlights the importance of properly choosing k based on the construction of the classification library. For all other testing parameters, the accuracy rate is consistently above 90%, with accuracy rates above 95% in the majority of runs. The high accuracy rate over a broad set of parameters indicates a well-performing wake detection protocol. The strong performance

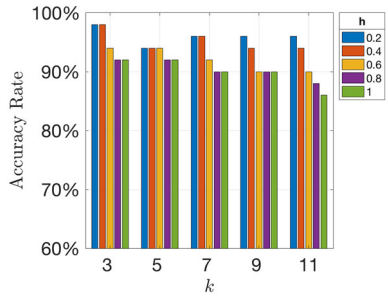

Fig. 15 Accuracy rate decreases with increasing separation distance h as well as with increasing number of nearest neighbors k. In all cases, the accuracy rate is above 85%

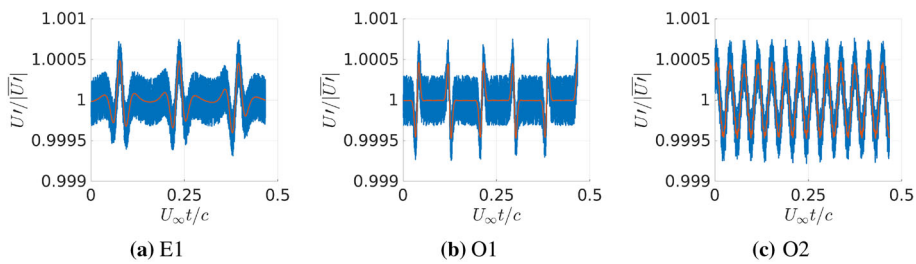

Fig. 16 Representative wake signatures with SNR = 3. Signatures are generated by 2P wakes with $\gamma = 3/7$ and $\mathcal{P} = -0.803$. Tiles (**a**–**c**) correspond to $\mathcal{H} = -0.2$, 0.4, and 0.13, respectively. The red curves are the original signals, and the blue curves are the noise-corrupted signals (colour figure online)

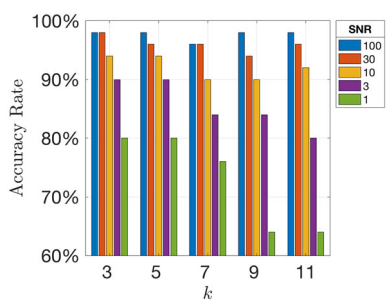

Fig. 17 Accuracy rate decreases with decreasing SNR. Additionally, as SNR decreases, the accuracy rate becomes more sensitive to the number of nearest neighbor points k. Results here are based on 50 test signals from randomly generated wakes using a classification library with 150 entries

here can be attributed to a suitable feature extraction method, which was informed by a close examination of representative wake signatures during the data collection and library construction process.

Beyond parameters associated with the wake detection protocol itself, other parameters—such as measurement noise and the separation distance h—can also influence the performance of the protocol, and will be considered now. To investigate the role of the separation parameter h, we repeat the library construction and wake detection study above, but now for a set of different separation values $h = \{0.2, 0.4, 0.6, 0.8, 1\}$. Figure 14 shows the results for $h = 0.4$ and $h = 0.8$. As seen in Fig. 15, accuracy rate decreases with increasing h. Examination of the wake classification library in Fig. 14 reveals that the 2P sub-regimes begin to blend together in feature space with increasing h, making the distinction between $E1$, $O1$, and $O2$ wakes more and more difficult. Interestingly, the 2S and 2P clusters remain well separated as h increases, and thus wake types remain distinguishable with larger separation distance.

Of course, the hydrodynamic signals imparted on the body will become weaker as h increases, and so will require more sensitive sensors to detect the faint velocity fluctuations associated with distant wake vortices. The sensors required for detecting the smaller velocity fluctuations imparted by distant wakes would inherently be more sensitive to sensor noise as well, which has the potential to adversely influence feature extraction and classification performance. Here, we investigate the influence of measurement noise on classification per-

formance by introducing a synthetic additive noise signal to the time-series measurements. Specifically, we study performance in the face of additive, independent and identically distributed zero-mean Gaussian noise over a range of intensity levels. Here, the intensity of the noise environment is quantified in terms of the signal-to-noise ratio (SNR), defined as the ratio of the magnitude of the mean to the standard deviation of the measured signal. A large SNR corresponds to a low-noise environment, whereas a small SNR corresponds to a high-noise environment. Figure 16 shows representative noise-contaminated signals with SNR $= 3$. We study the protocol for SNR $= \{1, 3, 10, 30, 100\}$, in each instance considering classification performance using 50 noisy test signals. The accuracy rates for different SNR levels are reported in Fig. 17. For low-noise environments (high SNR), the number of k nearest neighbors has negligible influence on the accuracy rate. For high-noise environments, accuracy rate decreases for any given k. Further, for SNR less than 10, the accuracy rate decreases with increasing number of k nearest neighbors. These observations indicate that in high-noise environments, protocol performance can be improved by choosing a smaller number of nearest neighbors. Even for SNR$= 1$, the classification accuracy rate can reach $\geq 70\%$ with a proper choice of k.

5 Discussion and conclusions

The results of the present study serve as a proof-of-concept demonstration for the viability of exotic wake detection based on hydrodynamic signals. A dynamic wake model was combined with a vortex panel method to study the hydrodynamic signatures imparted by various dynamically distinct wake regimes on a fish-like body. We found that different wake regimes impart distinct hydrodynamic signatures whose qualitative differences can be detected in time-series measurements taken at a single point on a fish-like body. Further, we found that the ability to detect these qualitative differences was insensitive to the sensor location.

An examination of wake signatures in the frequency domain revealed that a Gaussian bell curve—defined by the parameters (μ, a, σ)—could be fit to the frequency signature to provide a concise summary of the wake as a feature vector. Subsequently, feature vectors from a wide range of wake regimes were collected and stored for use in a wake classification library. After doing so, we invoked the k-nearest neighbor algorithm to compare the signatures from unknown wake regimes with entries in the wake classification library. The performance of this wake detection protocol was assessed by considering the accuracy over a range of algorithmic parameters; this assessment study showed that the wake detection protocol performed with an accuracy rate of over 95% for a majority of algorithm parameter values. The notable performance of the wake detection method over a wide range of algorithm parameters indicates that the feature extraction approach was appropriate for summarizing the wake signatures; indeed, the ability of the wake detection protocol to reliably distinguish between wake regimes shows that the feature vectors effectively captured the primary qualitative distinctions between signatures from dynamically distinct wakes. The results of this proof-of-concept study indicate that future investigations moving beyond the ideal fluids models considered here will benefit from determining appropriate feature vectors for the given context.

One challenge we observed was an inability to reliably distinguish between wake signatures with wake dynamics evolving near regime boundaries. A closer inspection of the "failure cases" in the performance assessment revealed difficulties in distinguishing between wake regimes that evolved close to the separatrices in phase space. Indeed, these were the same wake regimes that had similar feature vectors to one another and were more closely clustered together in the classification library. This observation suggests that even with a richly populated library, the wake detection accuracy rate is unlikely to reach 100%. Further, this suggests that other wake regimes not studied here—such as the mixed regime reported in [4] that exhibit qualities of both orbiting and exchanging regimes—may require special consideration when devising a wake detection protocol.

The influence of sensor noise and separation distance on classification performance were also investigated. Sensor noise was studied over a range of SNR levels. Although low SNR degraded performance in general, we found that classification accuracy can be improved by choosing a relatively small number k of nearest neighbors in the algorithm. Additionally, the influence of separation distance h on classification performance was studied. As the separation distance h was increased, the features associated with 2P sub-regimes were found to become less distinct and to blend with one another. Overall classification accuracy decreased with increasing h; however, the distinction between 2S and 2P wake types remained clear in feature space for up to a full body length of separation.

We note that the study here demonstrates the viability of using hydrodynamic signals to detect and classify wakes in an idealized setting; much work remains to be done to demonstrate the viability of doing the same in the

face of numerous practical real-world challenges. In the present study, numerous constraints were imposed—both on the wake parameters and on the relative location and orientation of the body-wake system—in order to demonstrate the viability of classifying wakes from their hydrodynamic signatures. In future investigations, wake classification libraries will need to be constructed with a richer set of entries that incorporate factors such as the relative alignment of the wake and body as well as the two-way coupling of hydrodynamic interactions between the two. Further, only velocity measurements taken at a single point on the body were considered here, which could limit the ability of wake detection protocol to distinguish between wake-generating systems. For example, at a sufficient distance, a 2P wake and 2S wake will impart strikingly similar hydrodynamic signatures.

In addressing these practical challenges, we can draw inspiration from biology once again. For example, the lateral line system is composed of arrays of both superficial and canal neuromasts, giving marine swimmers access to a multimodal and distributed sensing system. Indeed, multimodal distributed sensing will be more likely to succeed at distinguishing between wakes when body-wake alignment and separation are unknown and need to be accounted for. Moreover, measurements of pressure and pressure gradients—as in canal neuromasts—may serve to amplify hydrodynamic signals and yield improved performance. It may also be possible to devise swimming gaits that are optimized for wake sensing and detection. Recent studies of biological swimmers show that properly timed head motions can lead to a threefold sensitivity of the lateral line system without compromising other performance objectives, such as propulsive efficiency [1]. Certainly, distributed and multimodal sensing combined with sensing-optimized gaits will play a role in making wake detection protocols more practically relevant for use in bioinspired robotic swimmers in the future.

References

1. Akanyeti, O., Thornycroft, P.J.M., Lauder, G.V., Yanagitsuru, Y.R., Peterson, A.N., Liao, J.C.: Fish optimize sensing and respiration during undulatory swimming. Nat. Commun. **7**, 11044 (2016). https://doi.org/10.1038/ncomms11044
2. Aref, H., Stremler, M.A., Ponta, F.L.: Exotic vortex wakes–point vortex solutions. J. Fluids Struct. **22**(6–7), 929–940 (2006). https://doi.org/10.1016/j.jfluidstructs.2006.04.015
3. Arnold, G.P.: Rheotropism in fishes. Biol. Rev. **49**(4), 515–576 (1974). https://doi.org/10.1111/j.1469-185X.1974.tb01173.x
4. Basu, S., Stremler, M.A.: On the motion of two point vortex pairs with glide-reflective symmetry in a periodic strip. Phys. Fluids **27**(10), 103603 (2015)
5. Bishop, C.M.: Pattern Recognition and Machine Learning. Springer, Berlin (2006)
6. Bleckmann, H.: Reception of Hydrodynamic Stimuli in Aquatic and Semiaquatic Animals, Progress in Zoology, vol. 41. Gustav Fischer Verlag, New York (1994)
7. Bleckmann, H., Zelick, R.: Lateral line system of fish. Integr. Zool. **4**(1), 13–25 (2009)
8. Borazjani, I., Sotiropoulos, F.: Numerical investigation of the hydrodynamics of carangiform swimming in the transitional and inertial flow regimes. J. Exp. Biol. **211**(10), 1541–1558 (2008)
9. Bouffanais, R., Weymouth, G.D., Yue, D.K.: Hydrodynamic object recognition using pressure sensing. In: Proceedings of the Royal Society of London A: Mathematical, Physical and Engineering Sciences, p. rspa20100095. The Royal Society (2010)
10. Chambers, L., Akanyeti, O., Venturelli, R., Ježov, J., Brown, J., Kruusmaa, M., Fiorini, P., Megill, W.: A fish perspective: detecting flow features while moving using an artificial lateral line in steady and unsteady flow. J. R. Soc. Interface **11**(99), 20140467 (2014)
11. Colvert, B., Kanso, E.: Fishlike rheotaxis. J. Fluid Mech. **793**, 656–666 (2016). https://doi.org/10.1017/jfm.2016.141
12. Cottet, G.H., Koumoutsakos, P.D.: Vortex Methods: Theory and Practice. Cambridge University Press, New York (2000)
13. DeVries, L., Lagor, F.D., Lei, H., Tan, X., Paley, D.: Distributed flow estimation and closed-loop control of an underwater vehicle with a multi-modal artificial lateral line. Bioinspiration Biomim. **10**(2), 025002 (2015). https://doi.org/10.1088/1748-3190/10/2/025002
14. Franosch, J.M.P., Hagedorn, H.J.A., Goulet, J., Engelmann, J., Van Hemmen, J.L.: Wake tracking and the detection of vortex rings by the canal lateral line of fish. Phys. Rev. Lett. **103**(7), 1–4 (2009). https://doi.org/10.1103/PhysRevLett.103.078102
15. Gemmell, B.J., Adhikari, D., Longmire, E.K.: Volumetric quantification of fluid flow reveals fish's use of hydrodynamic stealth to capture evasive prey. J. R. Soc. Interface **11**(90), 20130880 (2014). https://doi.org/10.1098/rsif.2013.0880
16. Hemati, M.S.: Learning wake regimes from snapshot data. In: AIAA Paper 2016-3781. 46th AIAA Fluid Dynamics Conference, AIAA Aviation, Washington, DC (2016)
17. Katz, J., Plotkin, A.: Low-Speed Aerodynamics, 2nd edn. Cambridge University Press, New York (2001)
18. Kern, S., Koumoutsakos, P.: Simulations of optimized anguilliform swimming. J. Exp. Biol. **209**(24), 4841–4857 (2006)
19. Klein, A., Bleckmann, H.: Determination of object position, vortex shedding frequency and flow velocity using artificial lateral line canals. Beilstein J. Nanotechnol. **2**(1), 276–283 (2011). https://doi.org/10.3762/bjnano.2.32
20. Lentink, D., Muijres, F.T., Donker-Duyvis, F.J., van Leeuwen, J.L.: Vortex-wake interactions of a flapping foil that models animal swimming and flight. J. Exp. Biol. **211**(Pt 2), 267–273 (2008). https://doi.org/10.1242/jeb.006155
21. Liao, J.C., Beal, D.N., Lauder, G.V., Triantafyllou, M.S.: Fish exploiting vortices decrease muscle activity. Science **302**, 1566–1569 (2003)

22. Marras, S., Killen, S.S., Lindström, J., McKenzie, D.J., Steffensen, J.F., Domenici, P.: Fish swimming in schools save energy regardless of their spatial position. Behav. Ecol. Sociobiol. **69**, 219–226 (2015)
23. Montgomery, J.C., Coombs, S., Baker, C.F.: The mechanosensory lateral line system of the hypogean form of astyanax fasciatus. Environ. Biol. Fishes **62**(1), 87–96 (2001). https://doi.org/10.1023/A:1011873111454
24. Moored, K.W., Dewey, P.A., Smits, A.J., Haj-Hariri, H.: Hydrodynamic wake resonance as an underlying principle of efficient unsteady propulsion. J. Fluid Mech. **708**, 329–348 (2012)
25. Müller, U.K., van den Boogaart, J.G.M., van Leeuwen, J.L.: Flow patterns of larval fish: undulatory swimming in the intermediate flow regime. J. Exp. Biol. **211**(Pt 2), 196–205 (2008). https://doi.org/10.1242/jeb.005629
26. Newton, P.K.: The N-Vortex Problem: Analytical Techniques. Springer, New York (2001)
27. Pitcher, T.J., Partridge, B.L., Wardle, C.S.: A blind fish can school. Science (New York, N.Y.) **194**(4268), 963–965 (1976). https://doi.org/10.1126/science.982056
28. Pohlmann, K., Grasso, F.W., Breithaupt, T.: Tracking wakes: the nocturnal predatory strategy of piscivorous catfish. Proc. Natl. Acad. Sci. **98**(13), 7371–7374 (2001). https://doi.org/10.1073/pnas.121026298
29. Ren, Z., Mohseni, K.: A model of the lateral line of fish for vortex sensing. Bioinspiration Biomim. **7**(3), 036016 (2012). https://doi.org/10.1088/1748-3182/7/3/036016
30. Saffman, P.: Vortex Dynamics. Cambridge University Press, New York (1992)
31. Schnipper, T., Andersen, A., Bohr, T.: Vortex wakes of a flapping foil. J. Fluid Mech. **633**, 411–423 (2009)
32. Sichert, A.B., Bamler, R., van Hemmen, J.L.: Hydrodynamic object recognition: when multipoles count. Phys. Rev. Lett. **102**(5), 058104 (2009)
33. Smits, A.J., Moored, K.W., Dewey, P.A.: Fluid-structure-sound interactions and control. In: Proceedings of the 2nd Symposium on Fluid-Structure-Sound Interactions and Control, Chap. The Swimming of Manta Rays, pp. 291–300. Springer, Berlin (2014). https://doi.org/10.1007/978-3-642-40371-2_43
34. Spedding, G.R.: Wake signature detection. Annu. Rev. Fluid Mech. **46**, 273–302 (2014)
35. Stremler, M.A.: Relative equilibria of singly periodic point vortex arrays. Phys. Fluids **15**(12), 3767–3775 (2003)
36. Stremler, M.A.: On relative equilibria and integrable dynamics of point vortices in periodic domains. Theor. Computat. Fluid Dyn. **24**(1), 25–37 (2010)
37. Stremler, M.A., Basu, S.: On point vortex models of exotic bluff body wakes. Fluid Dyn. Res. **46**(6), 061410 (2014). https://doi.org/10.1088/0169-5983/46/6/061410
38. Stremler, M.A., Salmanzadeh, A., Basu, S., Williamson, C.H.K.: A mathematical model of 2P and 2C vortex wakes. J. Fluids Struct. **27**(5–6), 774–783 (2011). https://doi.org/10.1016/j.jfluidstructs.2011.04.004
39. Tan, P.N., Steinbach, M., Kumar, V.: Introduction to Data Mining. Pearson, Boston (2006)
40. Triantafyllou, M.S., Weymouth, G.D., Miao, J.: Biomimetic survival hydrodynamics and flow sensing. Annu. Rev. Fluid Mech. **48**(1), 150720185944007 (2016). https://doi.org/10.1146/annurev-fluid-122414-034329
41. Tytell, E.D., Borazjani, I., Sotiropoulos, F., Baker, T.V., Anderson, E.J., Lauder, G.V.: Disentangling the functional roles of morphology and motion in the swimming of fish. Integr. Comp. Biol. **50**(6), 1140–1154 (2010)
42. Wang, M., Hemati, M.: Classifying exotic wakes with a flow speed sensor. In: AIAA Paper, pp. 2018–1289 (2018)
43. Weihs, D., Webb, P.: Optimal avoidance and evasion tactics in predator–prey interactions. J. Theor. Biol. **106**(2), 189–206 (1984). https://doi.org/10.1016/0022-5193(84)90019-5
44. Williamson, C., Roshko, A.: Vortex formation in the wake of an oscillating cylinder. J. Fluids Struct. **2**(4), 355–381 (1988)
45. Windsor, S.P., Norris, S.E., Cameron, S.M., Mallinson, G.D., Montgomery, J.C.: The flow fields involved in hydrodynamic imaging by blind mexican cave fish (astyanax fasciatus). part i: open water and heading towards a wall. J. Exp. Biol. **213**(22), 3819–3831 (2010). https://doi.org/10.1242/jeb.040741
46. Windsor, S.P., Norris, S.E., Cameron, S.M., Mallinson, G.D., Montgomery, J.C.: The flow fields involved in hydrodynamic imaging by blind mexican cave fish (astyanax fasciatus). part ii: gliding parallel to a wall. J. Exp. Biol. **213**(22), 3832–3842 (2010). https://doi.org/10.1242/jeb.040790

Publisher's Note Springer Nature remains neutral with regard to jurisdictional claims in published maps and institutional affiliations.